International Journal of Concrete Structures and Materials

RESEARCH Open Access

Investigation on the Micro-Grinding Induced Crystallographic Variations of Nine Different Clinkers

Hyunuk Kang[1], Jihoon Lee[1], Jun-Boum Park[1,2] and Juhyuk Moon[1,2*]

Abstract

Although clinker has been used for many years, complicated mineralogical properties of clinker pose challenges for the precise quantification. In this study, the mineralogical and crystallographic properties of nine different clinkers according to grinding procedures were investigated. With the dry-grinding for 2 h, particle size reduction to 3 μm of median particle size with a substantial phase transition to an amorphous phase observed, to which alite (C_3S) mainly contributed to the transition. Meanwhile, the crystallographic properties of the clinker phases were barely changed during the wet-grinding. In the wet-grinding program, the amount of ferrite solid solution (C_4AF) with a high linear absorption coefficient was not underestimated. Furthermore, well-corrected preferred orientation effect on C_3S was positively contributed to the analysis result of clinkers with the wet-grinding. Hence, it was suggested that the crystallographic effects observed in the wet-grinding program could produce more reliable results in phase analysis for the clinkers.

Keywords X-ray powder diffraction method, Grinding program, Clinker, Alite, Amorphous phase

1 Introduction

Worldwide, approximately 4 billion tons of Portland Cement (PC) is being consumed every year because of its suitable material performance and price competitiveness (Alyaseen et al., 2023; Bamigboye et al., 2020; Li et al., 2003; Shah et al., 2023; Tran et al., 2023). PC consists of various minerals, such as alite (C_3S), belite (C_2S), aluminate (C_3A) and ferrite solid solution (C_4AF). The type of cement varies and is classified based on the content of clinker phases. Depending on the relative contents of these minerals, the material properties of PC develop differently (Miller, 2018; Xie & Visintin, 2018). Hence, the minerals present in cement should be thoroughly calculate to design the performance of cement-based materials. For instance, to understand the mineralogical characteristics and hydration of cement, thermogravimetric analysis, nuclear magnetic resonance, and X-ray powder diffraction (XRPD) techniques have been actively utilised (Alarcon-Ruiz et al., 2005; Hesse et al., 2011; Naik et al., 2006; Parry-Jones et al., 1988). Amongst them, XRPD is one of the most adopted methods for analysing the mineralogical properties of PC (Goergens et al., 2020; Scarlett et al., 2001; Scrivener et al., 2004).

For the optimal investigation of XRPD, various factors must be considered, such as measurement condition, analysis method, and sample preparation. The adequate measurement conditions including X-ray scanning range, spinning speed, type of slit, maximum sample thickness, and step size should be determined empirically or theoretically (Wang, 1994; Whitfield & Mitchell, 2009). One analysis method, the Rietveld refinement method, is

Journal information: ISSN 1976-0485 / eISSN 2234-1315.

*Correspondence:
Juhyuk Moon
juhyukmoon@snu.ac.kr
[1] Department of Civil and Environmental Engineering, Seoul National University, 1 Gwanak-Ro, Gwanak-Gu, Seoul 08826, Republic of Korea
[2] Institute of Construction and Environmental Engineering, Seoul National University, 1 Gwanak-Ro, Gwanak-Gu, Seoul 08826, Republic of Korea

used to quantify the crystalline and amorphous phases combined with the internal standard or external standard method. If the amorphous phase is contained in the powder, then the crystalline and amorphous content can be indirectly quantified with the known information of a standard material (Fiebich & Mutz, 1999; Phillips, 1997; Scarlett et al., 2002; Shafi et al., 1997; Young, 1993). Accordingly, various discussion and proposals on the optimal measurement conditions and subsequent analysis method for quantitative XRPD (QXRPD) have been reported (Brindley, 1945; De la Torre & Aranda, 2003; Taylor et al., 2002; Whitfield & Mitchell, 2009).

Likewise, the effect of the particle size distribution in XRPD analysis has been also investigated (Gordon & Harris, 1955; Mitchell et al., 2007; Taylor et al., 2002; Whitfield & Mitchell, 2009). A large particle size could introduce errors into the XRPD pattern, which is closely related to the large crystallite size and the poorly refined preferred orientation (Dongxu et al., 2000; Ermolovich & Ermolovich, 2016; Kumar et al., 2004; Mejdoub et al., 2017). If the linear absorption coefficient of the specific crystalline phase is higher than those of the other phases, then the phase content of the phase can be underestimated (Guirado et al., 2000; Peterson et al., 2006). In addition, it was reported that larger particle size of clinker may yield the different shapes of patterns for identical measurement. Therefore, the patterns would not be able to be well-unified (Whitfield & Mitchell, 2009). Therefore, the accuracy of the XRPD analysis is highly affected by the particle size distribution of the powder. Recently, research has investigated whether the amorphous phase is contained in ordinary Portland Cement (PC), focusing on the factors mentioned above (León-Reina et al., 2009; Suherman et al., 2002; Walenta & Füllmann, 2004). Torre et al. reported that a remarkable amount of amorphous content was found in PC. Using the QXRPD technique combined with the internal standard method, the amount of the amorphous phase was calculated. And, to identify the degree of error, the amount of contained internal standard powder and the scan range of the XRPD pattern were assigned to experimental parameters. It was concluded that PC and clinker contained significant amounts of amorphous content (De la Torre et al., 2001). However, Jensen et al. conducted investigations into the effect of the physical properties of C_3S in QXRPD analysis. In addition, the reliability of QXRPD combined with the internal standard and external standard methods was discussed. It was concluded that amorphous content was not found in PC (Jansen et al., 2011). Furthermore, the effect of the particle size distribution of powder was investigated by Snellings et al. (). To verify the reliability of the QXRPD results, Snellings and colleagues adopted the external and internal standard methods, and two types of software (i.e. Highscore and TOPAS software) for QXRPD were employed to cross-check the results: but the significant differences were not confirmed. It has been also reported that the amorphous content was not included in the investigated PC in the study.

As summarised above, there is a still active debate on the nature of amorphous phase in PC. It is due to the analytical complexity of QXRPD and material uncertainty or variability of PC. To elucidate the issue, nine as-received clinkers (not PC) were investigated with two different programs of dry- and wet-grindings. It includes particle size analysis and the amount of the amorphous phase which was investigated by quantitative Rietveld analysis with the internal standard method. The increase of amorphous phase by the dry-grinding process was correlated with the decrease of certain mineral phase in the clinkers. The crystallographic difference in different grinding programs was interpreted with the degrees of preferred orientation of monoclinic C_3S (M3) and micro-absorption of C_4AF in the clinkers with different particle size.

2 Materials and Experimental Methods

Nine types of clinker were collected from different cement plants in the Republic of Korea. Clinker powders were pre-treated as follows. The acquired clinker nodules underwent an actual cement grinding process. In specific, the nodules were initially crushed in a roll crusher, a preliminary grinding process, without the addition of gypsum. Subsequently, the obtained coarse clinker powder was pulverised into a very fine powder using a cement ball mill, which is the main grinding facility. Last, pulverised homogeneous powder forms of clinkers were prepared with a Henschel mixer. Particle size distributions of the as-received clinkers will be compared with those of micro-ground clinker in Sect. 3.1. The X-ray fluorescence results (S8 Tiger, Bruker Co. Ltd., Land Baden-Württemberg, Germany) are presented in Table 1, with the loss of ignition (LOI) obtained from a weight loss percentage by heating at 1050 °C for 2 h. The variations were observed in Al_2O_3, Fe_2O_3, and MgO content according to the type of clinker. Al_2O_3 variations could be linked to both cooling rate and the addition of a significant Fe source. Discrepancies in Fe_2O_3 are likely due to variations of content of raw material, a crucial iron source in clinker production.

Dry- or wet-grinding programs were performed using lab-scale micro-ball mill equipment (XRD-Mill McCrone, Retsch Co. Ltd., Retsch-Allee, Germany) with a 125-mL jar and 48 cylindrical grinding balls were adopted for grinding clinker powders. Based on the preliminary experiments, 5 g of clinker was pulverised for 2 h for dry-grinding and methanol solution (6 mL) was

Table 1 X-ray fluorescence results for clinkers

Phase (unit %)	Clinker1	Clinker2	Clinker3	Clinker4	Clinker5	Clinker6	Clinker7	Clinker8	Clinker9
SiO_2	21.7	21.8	19.8	21.8	20.3	20.8	20.6	20.1	20.2
Al_2O_3	4.7	4.8	4.5	4.6	5.7	5.4	5.0	4.8	4.4
Fe_2O_3	3.7	3.3	3.2	3.5	3.5	3.3	3.2	4.0	3.2
CaO	63.5	63.7	63.5	64.5	63.6	64.0	63.4	63.0	63.3
MgO	2.4	3.5	4.0	2.8	2.5	4.1	4.2	4.7	5.4
SO_3	1.0	0.4	0.8	0.4	0.7	0.3	0.7	0.7	0. 6
K_2O	1.2	1.0	1.5	1.0	1.5	0.7	1.1	1.0	0.9
Na_2O	0.3	0.1	0.1	0.2	0.4	0.2	0.4	0.2	0.2
MnO	0.1	0.2	0.3	0.1	0.1	0.2	0.2	0.1	0.4
TiO_2	0.3	0.3	0.2	0.2	0.4	0.3	0.2	0.3	0.2
P_2O_5	0.3	0.2	0.5	0.1	0.4	0.2	0.2	0.4	0.4
SrO	0.1	–	0.1	0.1	0.1	–	0.1	0.1	0.1
LOI	0.9	0.75	1.6	0.8	0.9	0.7	0.8	0.8	1.1

added for wet-grinding program. In more detail, the grinding time was determined based on numerous preliminary experiments, set at the minimum duration where the preferred orientation effect of C_3S remains constant. After wet grinding, the powders were separated from methanol using a negative pressure machine and then dried for 40 min at 70 °C. The grinding durations were separated for 1 min after 10 min of grinding to prevent potential temperature rise. To measure the particle size distribution of the clinkers, the particle size analyser (Malvern Instrument Ltd., Malvern, UK) was used. Two measurements were taken per sample, and the measurements were made after achieving sufficient dispersion in isopropanol. The as-received clinker, dry-ground clinker, and wet-ground clinker are notated as ARC, DGC, and WGC, respectively.

XRPD patterns were measured with an X-ray diffractometer (D2 Phaser, Bruker Co. Ltd., Land Baden-Württemberg, Germany), and the obtained patterns are presented in Additional file 1: Figs. S1–S3. The device was equipped with Cu-Kα radiation (λ = 1.5418 Å), and the measurement range was set from 5° to 60° (2θ) with an optimal step size of 0.02° per 2θ. The generator voltage and the tube current were assigned to 30 kV and 10 mA, respectively (Jeong et al., 2020; Maheswaran et al., 2016). The goniometer radius used was 141 mm. To mitigate the effects of X-ray scattering at a low angle range, a slit with a size of 0.1 mm was inserted on the generator side. The clinker samples were rotated to improve particle statistics (Shi et al., 2017; Sun & Vollpracht, 2018).

TOPAS software version 7.0 (Bruker Co. Ltd., Land Baden-Württemberg, Germany) was used to conduct the QXRPD analysis of the clinkers. The clinkers were measured three times for one sample in the form of lightly pressed powder for assuring the reliability of measurement. The background of the XRPD pattern was determined with the Chebyshev polynomial function and 1/X term in the TOPAS software. The scale factors, lattice parameters, and full-width at half-maximum (FWHM) factors were carefully refined to stabilise the Rietveld refinement. In particular, except for the C_3S, C_2S, and C_4AF phases, the FWHM profile parameters were constrained with the value established in the previous literature (Chaix-Pluchery et al., 1987; De la Torre & Aranda, 2003; Hazen, 1976b; Mondal & Jeffery, 1975; Smyth, 1975). March-Dollase preferred orientation corrections were refined to the phases of C_3S (M3) and olivine (Dollase, 1986). The simulated diffraction patterns for ARC7 and WGC 7 are presented in Fig. 1a and b, respectively.

To quantify the exact amount of the crystalline phase and the amorphous phase contained in the clinkers, the internal standard method was adopted (Sakai et al., 2005; Shanahan & Zayed, 2007). The internal standard and the clinker samples were mixed with a specific weight ratio (internal standard reference: clinker powder = 1:9) by hand mixing for 30 min, with a mortar. The calibration process for the weight fractions was calculated according to Eqs. (1–2) (Guirado et al., 2000):

$$Corr(W_a) = W_a \frac{STD_{known}}{STD_{measured}} \tag{1}$$

$$W_{amorphous} = 1 - \sum Corr(W_x) \tag{2}$$

where $Corr(W_a)$, STD_{known}, $STD_{measured}$, and $W_{amorphous}$ represent the corrected weight percentage, weighed concentration of the standard, analysed concentration of the standard, and weight percentage of amorphous material, respectively. Zincite (NIST SRM 674b) was used

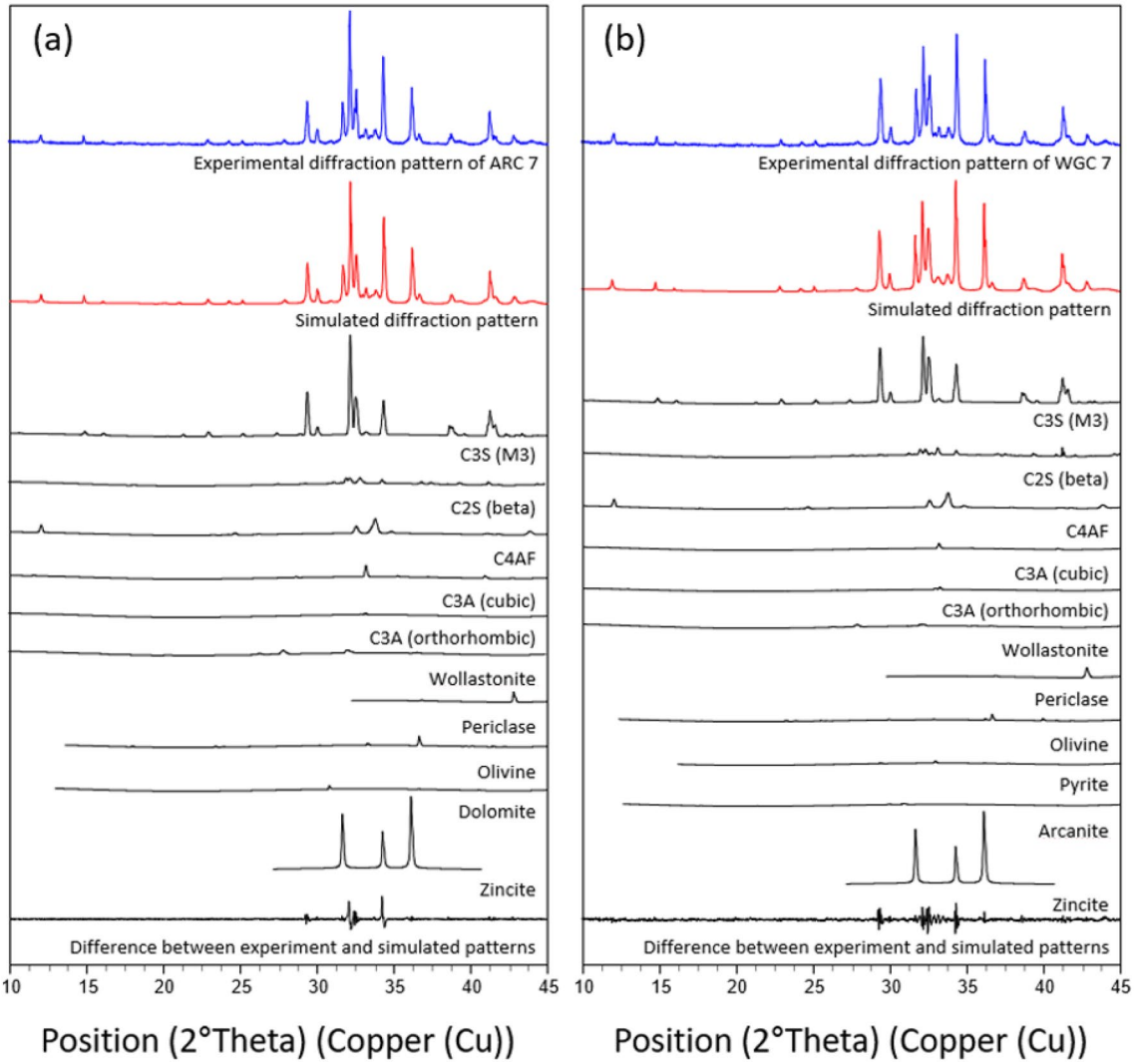

Fig. 1 Rietveld refinement result of XRPD pattern of ARC7 (**a**) and WGC 7 (**b**)

as the internal standard reference (Chrysochoou et al., 2010; Gualtieri et al., 2012; Snellings et al., 2010). The QXRPD results of ARC, DGC, and WGC are presented in Tables 2, 3, and 4, respectively.

Furthermore, the effect of inclusion of C_3S polymorphs (M3, triclinic [T1], and gamma [γ]) on the QXRPD analytical result of all samples of ARC, DGC, and WGC was investigated. Since the powder diffraction peaks corresponding to the C_3S polymorphs are severely overlapped in the 32.1˚ and 32.6˚ for 2θ, it is challenging to accurately identify the existence of minor C_3S polymorphs (T1 and γ) in the clinker (Bigare et al., 1967; Dunstetter et al., 2006; Jansen et al., 2011). Therefore, the minor C_3S polymorphs were generally excluded in qualitative XRPD analysis (Jansen et al., 2011; Snellings et al., 2014; Whitfield & Mitchell, 2009). However, in this study, QXRPD analysis has been conducted twice (i.e. with the minor C_3S polymorphs and without the polymorphs). The QXRPD analysis result without the minor C_3S polymorphs is shown in Tables 2, 3 and 4. The analytical results with the inclusion of C_3S polymorphs of T1 and γ have been presented in Additional file 1: Tables S1–S3.

3 Result and Discussion

3.1 Effects on the Particle Size Distribution of Clinker Powder According to Dry- or Wet-Grinding Program

The particle size distributions of all investigated clinkers are presented in Fig. 2(a-i). In the case of ARC, the particle size distribution is wider than the other samples. It was observed that the particle size range was between 3 μm and 395 μm, and it exhibited 2 peaks. Furthermore, the median particle size of ARC ranged from 20 μm to 60 μm. For the DGC samples, a narrow particle size distribution ranging from 1 μm to 8 μm was observed, with

Table 2 QXRPD analysis results of ARC

Phase (wt.%)	ARC1	ARC2	ARC3	ARC4	ARC5	ARC6	ARC7	ARC8	ARC9
Alite (M3) (Mumme, 1995)	56.2 (0.7)	51.3 (1.9)	62.2 (0.8)	58.9 (2.0)	55.4 (0.9)	56.4 (0.7)	44.7 (4.0)	41.6 (2.5)	54.5 (1.3)
Belite (Beta) (Mumme et al., 1995)	16.0 (1.8)	20.6 (0.4)	6.6 (0.2)	12.5 (0.7)	11.2 (1.6)	13.2 (1.3)	10.7 (1.4)	17.8 (0.0)	10.2 (0.6)
Ferrite (Colville & Geller, 1971)	13.5 (1.1)	13.0 (0.4)	13.6 (0.3)	13.1 (0.2)	11.5 (0.1)	11.5 (1.8)	9.2 (0.7)	12.2 (0.6)	10.1 (0.1)
Aluminate (cubic) (Mondal & Jeffery, 1975)	1.8 (0.4)	2.2 (0.2)	1.3 (0.0)	1.8 (0.2)	3.1 (1.1)	3.4 (0.0)	2.7 (0.2)	1.7 (0.2)	2.0 (0.0)
Aluminate (orthorhombic) (Nishi & Takeuchi, 1975)	1.1 (0.1)	1.0 (0.1)	–	0.6 (0.1)	1.5 (0.7)	–	0.4 (0.3)	–	–
Wollastonite (Yang & Prewitt, 1999)	2.9 (0.2)	2.8 (0.3)	3.8 (0.5)	4.5 (0.1)	1.7 (0.7)	5.1 (0.2)	2.9 (0.6)	3.4 (1.2)	4.1 (0.5)
Periclase (Hazen, 1976a)	1.1 (0.1)	3.0 (0.6)	6.0 (1.5)	1.4 (0.3)	1.7 (0.0)	3.5 (0.0)	3.4 (0.3)	3.9 (0.0)	4.7 (0.0)
Ca-ferrite (Lazić et al., 2006)	1.2 (0.1)	–	–	–	0.1 (0.0)	0.4 (0.4)	–	–	–
Hydrogrossular (Basso, 1983; Ferro et al., 2003)	1.1 (0.1)	1.6 (0.1)	1.6 (0.7)	0.9 (0.8)	3.0 (1.0)	1.5 (0.0)	0.1 (0.1)	1.3 (1.4)	1.2 (0.2)
Olivine (Hazen, 1976b; Smyth, 1975)	3.0 (0.1)	2.2 (0.9)	2.7 (0.3)	3.3 (0.3)	3.6 (0.4)	3.8 (0.1)	2.8 (0.7)	0.2 (0.2)	3.6 (0.1)
Dolomite (Steinfink & Sans, 1959)	0.2 (0.2)	0.3 (0.1)	0.3 (0.3)	0.3 (0.0)	1.0 (0.3)	0.4 (0.1)	0.3 (0.4)	0.7 (0.3)	–
Arcanite (McGinnety, 1972)	0.6 (0.1)	0.6 (0.1)	0.8 (0.2)	0.4 (0.1)	0.5 (0.2)	0.1 (0.0)	0.3 (0.2)	0.3 (0.1)	0.5 (0.0)
Pyrite (Bayliss, 1989; Buerger, 1937)	0.1 (0.0)	0.2 (0.2)	–	–	–	–	0.1 (0.1)	0.1 (0.0)	–
Syngenite (Corazza & Sabelli, 1967)	0.4 (0.0)	–	–	–	–	–	–	0.1 (0.1)	–
Portlandite (Chaix-Pluchery et al., 1987)	0.2 (0.2)	0.2 (0.0)	0.3 (0.3)	0.1 (0.1)	–	0.5 (0.1)	0.3 (0.1)	–	–
Amorphous	0.6 (0.1)	1.0 (3.9)	0.8 (1.5)	2.2 (2.7)	5.7 (0.4)	0.2 (1.2)	22.1 (7.0)	16.7 (0.8)	9.1 (1.2)
R_{wp}	10.1	9.9	10.0	10.1	10.5	9.7	9.8	8.6	10.1

The averaged weight percentage and standard deviation of three analysed results are presented

a median particle size of about 3 μm. Meanwhile, in the case of the WGC sample, a broad particle size distribution was observed, and two peaks were identified. However, a significant particle size reduction effect was noted when compared to that of the ARC. The median particle size for these samples was around 10 μm. Therefore, a substantial reduction in particle size was clearly confirmed in all clinkers, regardless of the type of grinding program.

Interestingly, differences were observed in the particle size depending on the type of grinding program (Fig. 3). The particle size distributions of the DGC were smaller than those of the WGC. This trend suggests that high-volume energy supplied by the ball mill can directly transfer to the clinker powder, and thus the particles could be finely pulverised with dry-grinding process. In addition, it should be noted here that the particle size distribution of the WGC was wider than that of the DGC (Fig. 2). In particular, in the case of the WGC, it was confirmed that there were significant amounts of particles between 0.2 μm and 1.0 μm, which indicated as a 2nd mode size (Figs. 2 and 3). This phenomenon might occur due to the difference in brittleness according to the type of clinker phase. In other words, it was shown that the particles containing a number of clinker phases with relatively low micro-structural stability were partially and more finely pulverised in a state of saturation with methanol (Le Saoût et al., 2011).

3.2 Qualitative X-ray Diffraction Analysis Results According to the Inclusion of C_3S Polymorphs

C_3S has known to have seven different polymorphs (i.e. M3, M2, M1, T3, T2, T1, and γ) (Bigare et al., 1967; Dunstetter et al., 2006). However, all the polymorphs are not usually considered in the QXRPD analysis with a medium resolution X-ray source (De Noirfontaine et al., 2006; Ren

Table 3 QXRPD analysis results of DGC

Phase (wt.%)	DGC1	DGC2	DGC3	DGC4	DGC5	DGC6	DGC7	DGC8	DGC9
Alite (M3) (Mumme, 1995)	38.5 (2.3)	42.0 (3.9)	46.2 (0.0)	47.9 (0.1)	41.5 (0.7)	39.1 (0.6)	42.5 (0.7)	36.5 (1.5)	45.0 (2.8)
Belite (Beta) (Mumme et al., 1995)	12.1 (1.9)	17.5 (4.5)	5.5 (1.6)	7.3 (0.0)	11.5 (0.6)	12.2 (0.5)	7.3 (0.5)	11.0 (0.9)	5.7 (0.1)
Ferrite (Colville & Geller, 1971)	10.5 (0.1)	11.5 (1.1)	10.1 (0.2)	10.2 (1.2)	9.1 (0.2)	10.8 (1.1)	8.2 (0.1)	10.8 (1.0)	7.8 (0.1)
Aluminate (cubic) (Mondal & Jeffery, 1975)	1.0 (0.2)	1.2 (0.2)	0.7 (0.2)	2.6 (0.8)	1.9 (0.3)	2.6 (0.2)	0.9 (0.1)	0.4 (0.4)	1.5 (0.3)
Aluminate (orthorhombic) (Nishi & Takeuchi, 1975)	0.3 (0.3)	0.5 (0.6)	0.9 (0.4)	0.7 (0.3)	1.4 (0.2)	1.2 (0.9)	1.1 (0.0)	0.5 (0.3)	1.0 (0.7)
Wollastonite (Yang & Prewitt, 1999)	2.0 (0.5)	2.4 (0.2)	2.0 (0.5)	3.5 (0.2)	2.2 (0.1)	2.6 (0.3)	1.9 (0.0)	2.8 (0.4)	1.5 (0.2)
Periclase (Hazen, 1976a)	0.8 (0.2)	1.5 (0.4)	2.5 (0.4)	0.6 (0.1)	1.1 (0.4)	2.6 (0.1)	2.5 (0.1)	3.2 (0.5)	3.6 (0.2)
Ca-ferrite (Lazić et al., 2006)	–	1.2 (0.4)	–	–	–	1.3 (0.3)	0.8 (0.2)	1.0 (0.0)	0.3 (0.3)
Hydrogrossular (Basso, 1983; Ferro et al., 2003)	2.1 (0.2)	0.5 (0.5)	1.2 (0.6)	1.8 (0.3)	3.5 (0.5)	–	1.3 (0.2)	0.5 (0.4)	0.9 (0.4)
Olivine (Hazen, 1976b; Smyth, 1975)	1.0 (1.1)	2.5 (0.1)	1.7 (0.3)	2.8 (0.1)	2.0 (0.3)	1.4 (0.0)	2.6 (0.0)	1.9 (0.0)	2.3 (0.2)
Dolomite (Steinfink & Sans, 1959)	0.8 (0.3)	0.6 (0.1)	0.5 (0.1)	0.5 (0.0)	1.1 (0.1)	0.4 (0.1)	–	0.1 (0.1)	0.4 (0.0)
Arcanite (McGinnety, 1972)	0.2 (0.1)	0.3 (0.1)	0.4 (0.0)	0.5 (0.1)	0.2 (0.1)	0.2 (0.1)	0.3 (0.0)	1.0 (0.0)	0.1 (0.1)
Pyrite (Bayliss, 1989; Buerger, 1937)	0.2 (0.1)	0.1 (0.0)	–	0.4 (0.1)	0.3 (0.1)	–	0.4 (0.1)	–	0.1 (0.1)
Syngenite (Corazza & Sabelli, 1967)	–	–	–	0.9 (0.1)	–	0.2 (0.2)	–	–	0.2 (0.2)
Portlandite (Chaix-Pluchery et al., 1987)	0.2 (0.2)	0.1 (0.1)	0.1 (0.1)	0.4 (0.0)	–	0.4 (0.0)	–	0.4 (0.1)	0.1 (0.1)
Amorphous	30.3 (2.4)	18.1 (10.7)	28.2 (3.1)	19.9 (0.5)	24.2 (1.3)	25.0 (1.1)	30.2 (0.6)	29.9 (2.9)	29.5 (5.2)
R_{wp}	9.9	9.2	10.2	10.0	10.1	9.3	9.4	10.1	9.7

The averaged weight percentage and standard deviation of three analysed results are presented

et al., 2017). Since not only some of C_3S (M3, T1, and γ) polymorphs were severely overlapped in the range of 32°–38°, but the patterns of two polymorphs of C_2S (beta [β] and gamma [γ]) also exist in that range. Therefore, it is challenging to quantify the existing amounts of the polymorphs of C_3S and C_2S. In this regard, the effect of the inclusion of C_3S polymorphs on the QXRPD result should be tested for optimal interpretation of subsequent measurements. From the conducted QXRPD of the all nine clinkers, the averaged values of weighted profile R-factor (R_{WP}) were compared in Fig. 4. When the calculated R_{WP} indices are about 10.0, it can be considered that the result of QXRPD is reliable (Toby, 2006). The calculated R_{WP} values of QXRPD considering three types of C_3S (M3, T1, and γ) were lower than that of QXRPD considering only one polymorph of C_3S (M3) for all three grinding conditions (ARC, DGC, and WGC). It shows that less accurately refined C_3S area can underestimate the total amount of C_3S compared to the case where only one polymorph was considered during the QXRPD analysis.

When the C_3S polymorphs (T1 and γ) are included in the QXRPD analysis, the amount of C_3S (γ) was quite high in the WGC (Table 4 and Additional file 1: Table S3). However, it was reported that the negligible amount of C_3S (γ) generally exists in a clinker owing to low thermodynamic stability at very high temperature (De Noirfontaine et al., 2006; Dunstetter et al., 2006). This abnormal phenomenon also led to underestimate the amount of C_2S. Simply, the overestimation of C_3S (γ) makes the actual amount of C_2S underestimated. Although the R_{WP} indices of QXRPD results without C_3S polymorphs were higher than those analysed with C_3S polymorphs, more reasonable results were derived when the C_3S polymorphs were excluded in the analysis. The higher R_{WP} value of the QXRPD results of WGC without C_3S

Table 4 QXRPD analysis results of WGC

Phase (wt.%)	WGC1	WGC2	WGC3	WGC4	WGC5	WGC6	WGC7	WGC8	WGC9
Alite (M3) (Mumme, 1995)	54.9 (0.2)	54.9 (0.8)	61.4 (0.7)	68.0 (0.3)	54.0 (1.2)	55.2 (1.0)	57.7 (2.2)	57.1 (0.3)	57.2 (1.0)
Belite (Beta) (Mumme et al., 1995)	17.3 (0.4)	12.5 (2.8)	3.6 (0.1)	3.9 (0.6)	11.3 (0.3)	10.5 (1.5)	8.3 (1.4)	12.5 (0.1)	6.2 (0.6)
Ferrite (Colville & Geller, 1971)	14.6 (1.9)	16.6 (0.4)	15.3 (0.4)	14.9 (0.9)	13.8 (0.4)	17.4 (1.1)	13.6 (1.1)	14.7 (0.1)	11.5 (0.0)
Aluminate (cubic) (Mondal & Jeffery, 1975)	1.5 (0.1)	0.8 (0.2)	3.7 (0.0)	2.6 (0.7)	3.0 (0.1)	3.4 (0.2)	2.6 (0.8)	0.7 (0.0)	2.3 (0.4)
Aluminate (orthorhombic) (Nishi & Takeuchi, 1975)	0.1 (0.1)	2.2 (0.2)	0.2 (0.1)	1.0 (0.2)	2.3 (0.1)	1.6 (0.3)	2.5 (0.8)	0.1 0.0	2.0 (0.3)
Wollastonite (Yang & Prewitt, 1999)	2.2 (0.1)	3.2 (0.8)	2.5 (0.0)	2.3 (0.7)	2.8 (0.3)	2.3 (0.2)	2.8 (0.3)	2.0 (0.0)	2.5 (0.3)
Periclase (Hazen, 1976a)	1.0 (0.0)	1.0 (0.4)	1.8 (0.0)	0.7 (0.0)	0.8 (0.1)	2.7 (0.3)	2.4 (0.3)	4.1 (0.0)	4.4 (0.0)
Ca-ferrite (Lazić et al., 2006)	2.3 (0.1)	2.4 (1.0)	3.4 (0.2)	1.1 (1.0)	1.0 (0.1)	0.9 (0.3)	1.7 (0.8)	1.3 (0.0)	4.6 (1.4)
Hydrogrossular (Basso, 1983; Ferro et al., 2003)	2.5 (0.1)	2.1 (0.7)	2.8 (0.0)	0.5 (0.2)	3.7 (0.8)	1.8 (0.4)	2.4 (0.0)	3.5 (0.0)	3.7 (0.0)
Olivine (Hazen, 1976b; Smyth, 1975)	2.4 (0.1)	0.4 (0.1)	0.8 (0.0)	1.4 (0.5)	0.4 (0.4)	0.3 (0.2)	0.8 (0.2)	1.8 (0.0)	1.7 (0.5)
Dolomite (Steinfink & Sans, 1959)	–	0.5 (0.4)	0.5 (0.0)	0.5 (0.2)	0.9 (0.3)	0.2 (0.1)	0.3 (0.1)	0.2 (0.0)	0.1 (0.1)
Arcanite (McGinnety, 1972)	0.4 (0.0)	1.0 (0.1)	1.4 (0.1)	0.3 (0.1)	0.6 (0.2)	0.1 (0.1)	1.0 (0.6)	0.2 (0.0)	0.6 (0.3)
Pyrite (Bayliss, 1989; Buerger, 1937)	–	1.0 (0.4)	1.8 (0.0)	0.4 (0.3)	1.4 (1.0)	0.3 (0.1)	0.2 (0.2)	–	0.6 (0.5)
Syngenite (Corazza & Sabelli, 1967)	–	0.4 (0.3)	–	0.8 (0.7)	1.8 (0.3)	0.2 (0.2)	1.2 (0.1)	0.2 (0.0)	0.2 (0.2)
Portlandite (Chaix-Pluchery et al., 1987)	0.3 (0.3)	0.9 (0.4)	0.5 (0.0)	1.5 (0.7)	2.1 (1.4)	1.7 (0.1)	1.9 (1.1)	0.7 (0.0)	0.9 (0.0)
Amorphous	0.5 (0.6)	0.1 (0.1)	0.3 (1.3)	0.1 (0.5)	0.1 (0.3)	1.4 (0.2)	0.6 (0.4)	0.9 (0.6)	1.5 (2.6)
R_{wp}	8.4	9.6	9.4	9.5	8.6	9.9	9.5	9.1	9.8

The averaged weight percentage and standard deviation of three analysed results are presented

polymorphs can be caused by the existence of incomplete C_3S (M3) superstructure (Courtial et al., 2003; De La Torre et al., 2002; Nishi et al., 1985; Snellings et al., 2014).

3.3 Effects of Dry- or Wet-Grinding Program on QXRPD Analysis

As can be seen in Fig. 5a, an unusually high C_3S peak was observed at 32.1° for 2θ in the XRPD pattern of the ARC, unlike in the previous studies (De La Torre et al., 2002; Mumme, 1995; Stutzman et al., 2016). It might be caused by the preferred orientation effect [i.e. reflected by a March-Dollase coefficient of 0.84 for all ARC of C_3S (M3)] originating from the large crystallite size of C_3S, in which the crystals were preferably developed in the [0 0 1] direction. It can yield a partial error in quantification of phases at the QXRPD analysis stage (De la Torre & Aranda, 2003; Snellings et al., 2014). As a result, the amorphous content calculated in the ARC using QXRPD ranges from 0.2 wt.% to 23.4 wt.% (Table 2). There was no correlation between particle size and the calculated amount of amorphous content in the ARC. To investigate micro-grinding effect on the mineralogical properties of clinkers, grinding time should be chosen. Based on several preliminary tests, it was confirmed that 2 h of grinding yield consistent amount of amorphous content in three identical measurements either by dry- or wet-grinding program.

The calculated amount of amorphous phase after 2 h of micro-grinding is presented in Fig. 6. A noticeable trend was observed depending on the selected grinding program. In the case of the DGC, the amount of amorphous phase substantially increased compared to the ARC case. On the other hand, it decreased to a negligible quantity in the WGC. These results can be explained as follows. When the dry-grinding program was additionally applied to the ARC for 2 h, it had a significant effect on the XRPD

measurement results. Overall, the intensity of almost all clinker phases got lower than those of the ARC (Fig. 5a). In particular, the intensity of one of the main peaks (32.1° of C_3S) was significantly reduced whilst the relative intensity was measured similarly as reported in the previous studies (Jansen et al., 2011; Stutzman et al., 2016). The reduction of the intensities of these XRPD peaks definitely affected the quantification analysis. The amount of amorphous phase surprisingly increased, which ranges from 18.7 wt.% to 30.9 wt.% (Fig. 6).

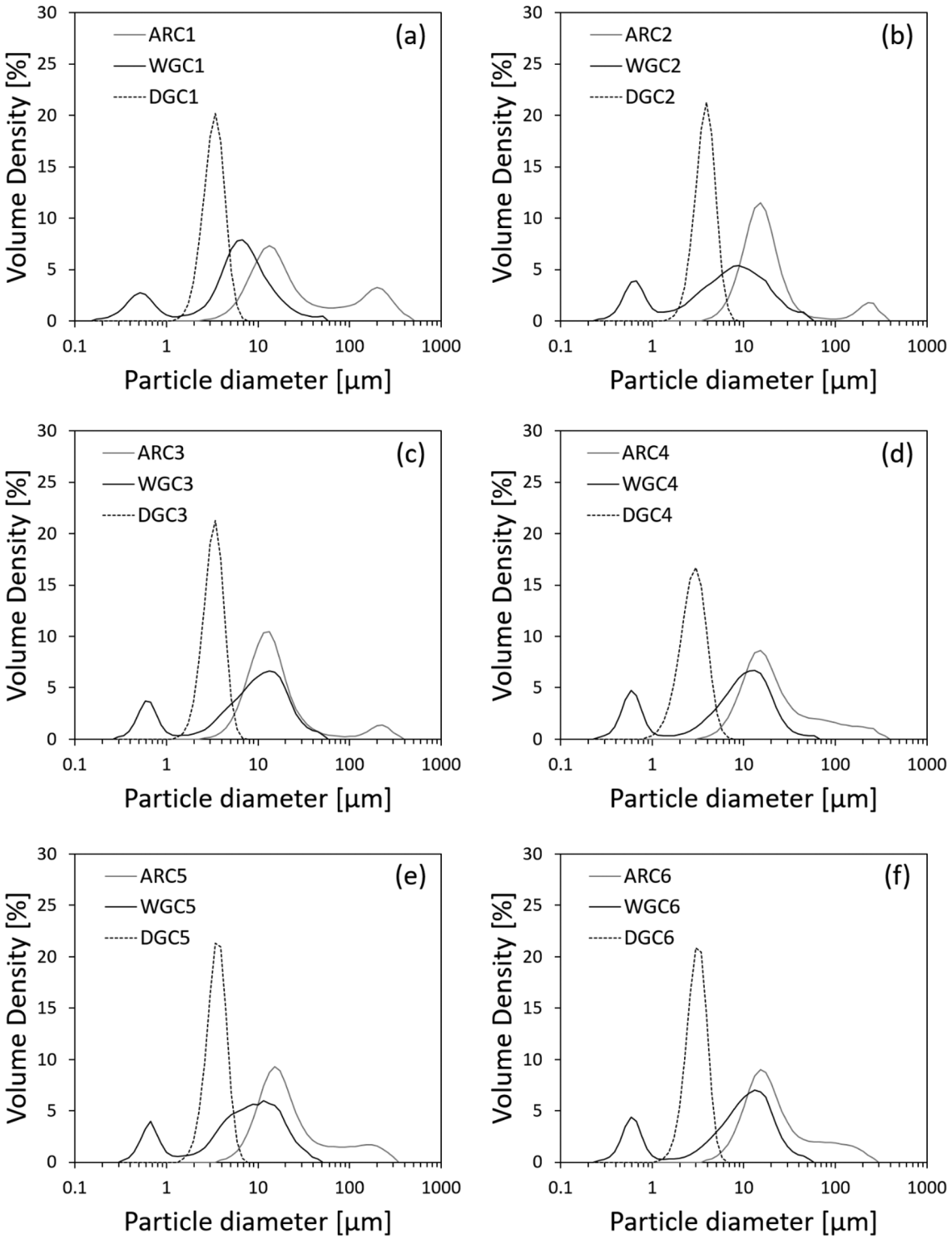

Fig. 2 Particle size distribution of the clinkers. ARC, WGC, and DGC indicate as-received clinker, wet ground clinker, and dry ground clinker, respectively

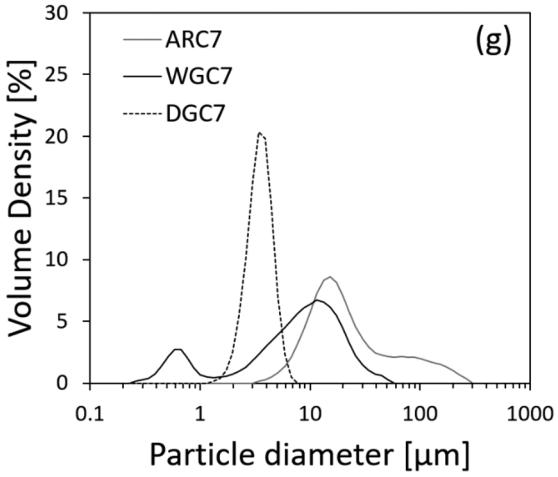

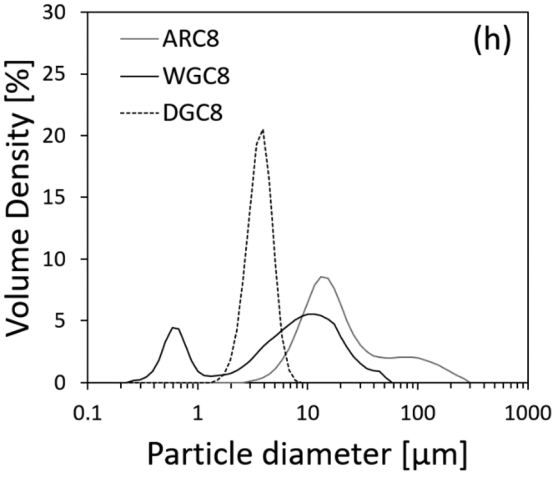

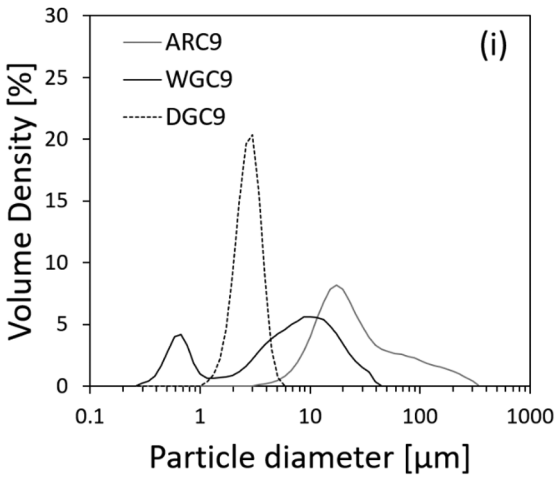

Fig. 2 continued

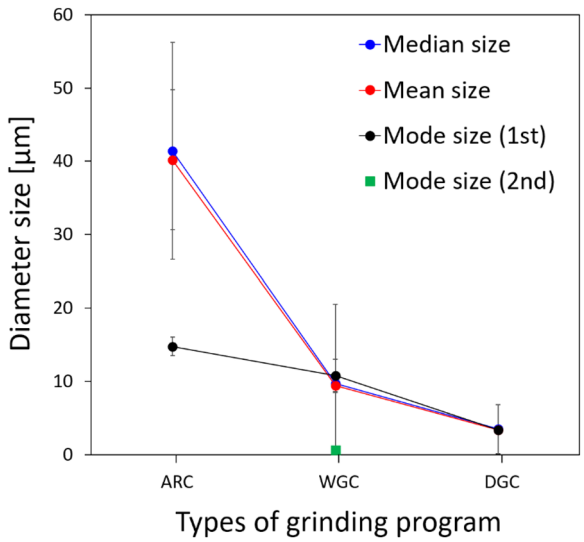

Fig. 3 Changes in the average and standard deviation of the particle size of the clinker according to grinding program

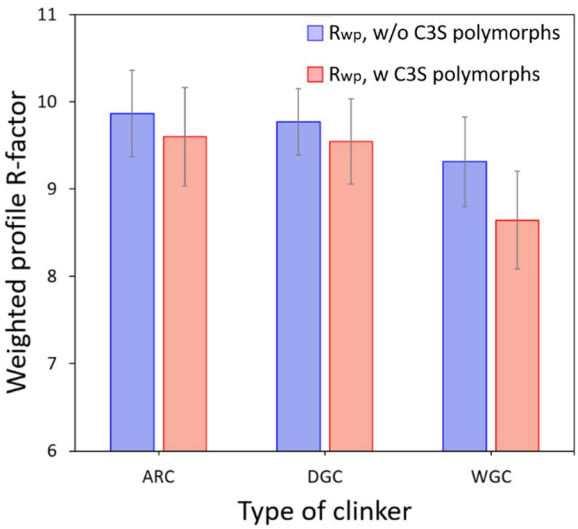

Fig. 4 Averaged weighted profile R-factor of QXRPD results

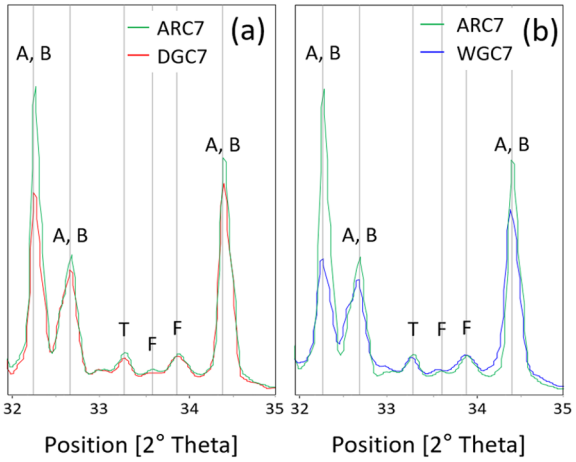

Fig. 5 Comparison of XRPD patterns of the ARC7 and DGC7 (**a**) and the ARC7 and WGC7 (**b**). Symbols A, B, F, and T represent C_3S, C_2S, C_4AF, and C_3A, respectively

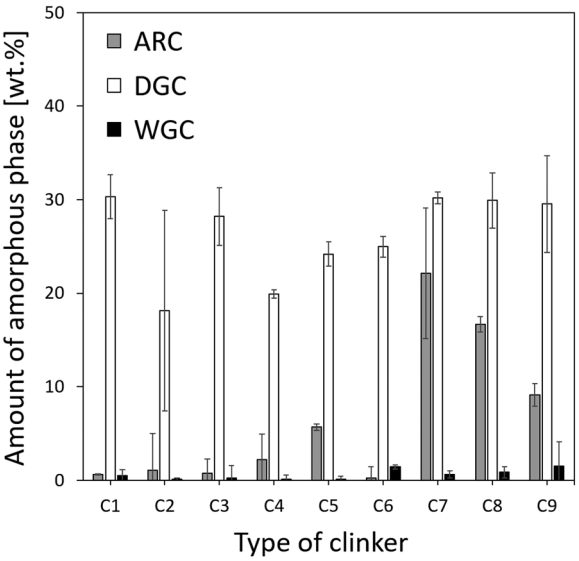

Fig. 6 Quantification of amorphous content according to the grinding programs

This result can be explained by not only applying the high-volume energy delivered by the ball mill to particle size reduction but also by partially modifying the crystallographic information of the clinker phases (Huang et al., 2017; Mejdoub, Hammi, Khitouni, Suñol, & M'nif, 2017). That is, crystallographic defects such as the dislocation and vacancies of atoms could arise during the dry-grinding program. These abnormal variations are sources that could change the crystalline phase to the amorphous phase (Dongxu et al., 2000; Juhász & Opoczky, 1990; Mejdoub, Hammi, Khitouni, Suñol, & M'nif, 2017; Snellings et al., 2014). In particular, it was confirmed that the increased amount of amorphous phase was remarkably correlated with the decreased amount of C_3S (Fig. 7). As the prolonged dry-grinding program was introduced, the preferred orientation of C_3S (M3) to the (0 0 3) plane was substantially reduced which could be confirmed by the increased March-Dollase coefficient value (i.e. fitted to 0.91 for DGC). Therefore, it is safe to conclude that C_3S, which has relatively lower spatial stability (Le Saoût et al., 2011), substantially contributed to the observed amorphisation of clinkers.

When wet-grinding program was applied to the ARC, well-corrected preferred orientation effect of C_3S was observed, and it was also confirmed by identically measured XRPD patterns for the same sample. The obtained March-Dollase coefficients for the ARC, DGC, and WGC were about 0.84, 0.91, and 0.96, respectively. In the case of WGC, the biased crystal growth with specific direction was hard to be observed (i.e. the fitted coefficient was almost close to 1.0 (Whitfield & Mitchell, 2009)). Furthermore, the broadness of the XRPD peaks of the WGC was wider than those of the ARC with lowered intensities. This result can be well-explained by the reductions of the particle size as well as the crystallite size of the clinker phases (Pourghahramani & Akhgar, 2015; Uvarov & Popov, 2007).

However, in the case of C_4AF (i.e. an interstitial mineral), the opposite result was observed by the wet grinding. When the crystallite size decreased, the peak broadened and as such the intensity should have been lowered. However, the intensity was measured to be rather high for the C_4AF. The obtained results originated from the high linear absorption coefficient of C_4AF (). Guirado et al., 2000; Peterson et al., 2006In the case of C_4AF, the linear absorption coefficient is high at about

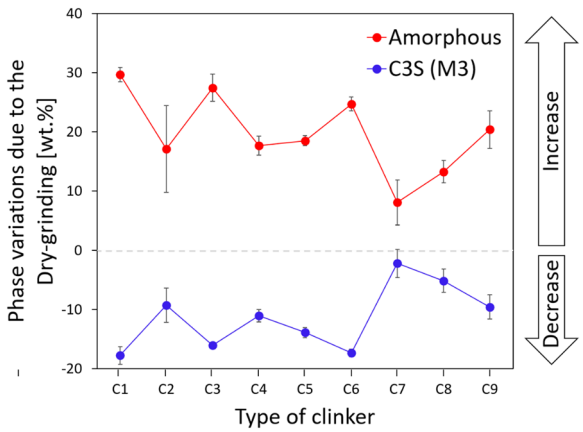

Fig. 7 Relation between C_3S and the amorphous phase according to the dry-grinding program

500 cm^{-1}, but for other clinker phases, it is mostly low at 300 cm^{-1}. Accordingly, in the case of C_4AF, which has a large crystallite size, the amount could be underestimated because it absorbs a relatively large amounts of irradiated X-rays. That is, the effect of reducing the degree of absorption of X-rays is more dominant than the effect of decreasing the peak intensity owing to the decrease in the crystallite size (De la Torre & Aranda, 2003). Therefore, the phenomenon observed in WGC (i.e. particle size reduction without causing the amorphisation effect), was possibly owing to the reduced preferred orientation of the C_3S (M3) phase, and the mitigated effect of linear absorption coefficient of C_4AF in finer size. Therefore, unlike the QXRPD analysis of the ARC and DGC, the amorphous content was substantially reduced in the results of the WGC (Fig. 8).

3.4 The Crystallographic Variations of C_3S (M3) and C_4AF Phases Induced by the Grinding Program

The averaged crystallite size can be calculated based on the value corresponding to the FWHM or the integral breadth of the XRPD peak. In general, as the peak intensity decreases and broadens, the crystallite size decreases (Pourghahramani & Akhgar, 2015; Uvarov & Popov, 2007). These shape changes of C_3S (M3) and C_4AF could be identified in Fig. 9a and b. More quantitatively, the variation of calculated FWHM by grinding program was analysed using peaks at 29.4˚ and 12˚ for C_3S (M3) and C_4AF, respectively (Fig. 9c). Under the dry-grinding program, no noticeable change of the FWHM was confirmed. However, the value of C_3S (M3) was significantly increased with the wet-grinding program. The increase in FWHM of C_3S (M3) indicated that the existing preferred orientation was appropriately corrected in the WGC, which had a bias concerning crystallinity in the

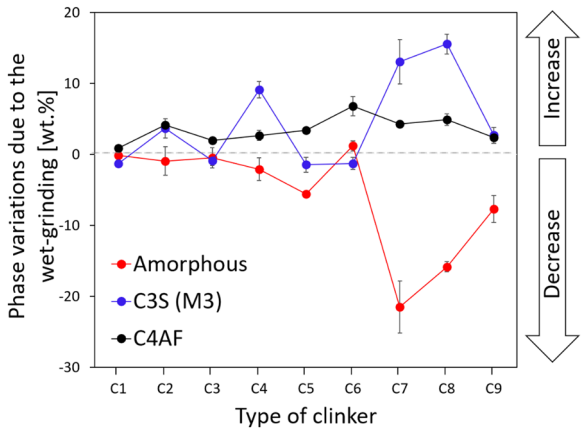

Fig. 8 Relation amongst C_3S, C_4AF and amorphous phases according to the wet-grinding program

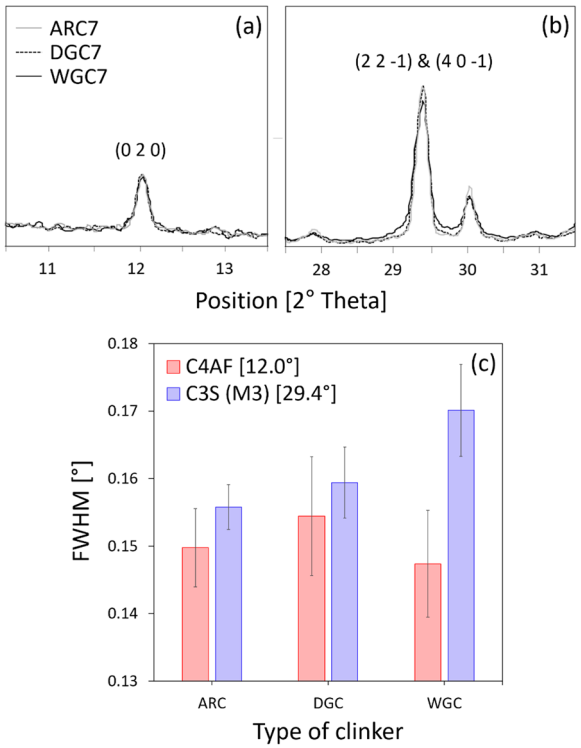

Fig. 9 Variations of C_4AF (**a**) and C_3S (M3) (**b**) peaks according to grinding program. Averaged value of FWHM of C_4AF and C_3S (M3) peaks (**c**)

[0 0 1] direction in ARC. On the other hand, the FWHM of C_4AF slightly increased in the DGC but decreased in WGC. The result of WGC found herein was not an effect normally caused by the grinding process (Pourghahramani & Forssberg, 2006; Radoi et al., 2004; Sheng et al., 2011). It can be explained by the micro-absorption coefficient of C_4AF. When the wet-grinding program was applied, the characteristics of X-ray absorption were significantly alleviated, and as a result, the decrease in particle size had a remarkable effect on the XRPD patterns (De la Torre & Aranda, 2003; Snellings et al., 2014). Therefore, unlike the C_3S (M3) phase, the C_4AF phase would not have been able to confirm the variations in the fine FWHM by the effect of pattern change due to the correction of micro-absorption by wet-grinding.

4 Conclusions

This study systematically investigated the nature of amorphous content in clinkers under different grinding programs, an issue still under debate. The relationship between the amorphous phase contained in the clinkers and the two types of grinding methodologies was covered through particle size measurement and QXRPD analysis. The conclusion of this study is as follows:

When the C_3S (M3, T1, and γ) polymorphs were included in the QXRPD analysis, the improved R_{WP} indices were obtained. In particular, it is mostly enhanced in the WGC. However, it was due to the misfitted C_3S (γ) when all C_3S polymorphs were included. It led to the overestimated amount of C_3S(γ) and unrealistic amount of C_2S. Therefore, it was proposed that QXRPD without considering the C_3S polymorphs is more reliable method and it was adopted for the subsequent analyses.

In the case of the DGC, the median particle size reduction to 3 μm resulted in a significant change in the QXRPD analysis results. It was confirmed that the intensity of the XRPD peaks was lowered, suggesting the amorphisation effect of clinker phases. In particular, a remarkable amorphisation effect of C_3S was confirmed.

Meanwhile, the wet-grinding program produced the median particle size of 10 μm. The correction of preferred orientation effect was supported by the crystallite size reduction of the C_3S (M3) phase in the WGC. In addition, the amount of C_4AF could be accurately calculated in the WGC owing to the particle size reduction. That is, the reduced degree of absorption of X-rays as the particle size decreases favourably contributed to the optimal estimation of C_4AF in WGC. There was negligible amount of amorphous phase estimated in the WGC. On the other hand, substantial amorphisation including C_4AF was observed in DGC and the amount of C_4AF was underestimated in ARC with large particle sizes.

The implementation of the method demonstrated in this study suggests that the wet-grinding program can be an adequate sample treatment methodology for obtaining more accurate mineralogical composition of clinker materials. In specific, it can lead to the negligible amount of amorphous phase and the more accurate estimation of C_4AF amount. Along with the application of this methodology to clinkers, it can be extended to quantitatively analyze the complex hydration reaction of PC especially focusing on the degree of reaction of C_3S and C_4AF.

Supplementary Information

The online version contains supplementary material available at https://doi.org/10.1186/s40069-024-00660-5.

Additional file 1: Fig. S1. X-ray diffraction patterns of ARC. **Fig. S2.** X-ray diffraction patterns of DGC. **Fig. S3.** X-ray diffraction patterns of WGC. **Table S1.** QXRPD analysis results of ARC considering C3S (T1 & r). The averaged weight percentage and standard deviation of three analysed results are presented. **Table S2.** QXRPD analysis results of DGC considering C3S (T1 & r). The averaged weight percentage and standard deviation of three analysed results are presented. **Table S3.** QXRPD analysis results of WGC considering C3S (T1 & r). The averaged weight percentage and standard deviation of three analysed results are presented.

Acknowledgements
This work was supported by Korea Institute of Energy Technology Evaluation and Planning (KETEP) grant funded by the Korea government (MOTIE) (20212010200080, Development of In situ carbonation technology using CO_2 released from cement industry). The Institute of Engineering Research at Seoul National University provided research facilities for this work.

Author Contributions
HK: conceptualisation, methodology, data curation, formal analysis, and writing original draft preparation. JL: methodology and data curation. JBP & JM: writing—reviewing and editing, and supervision.

Funding
This work was supported by Korea Institute of Energy Technology Evaluation and Planning (KETEP) grant funded by the Korea government (MOTIE) (20212010200080, Development of in-situ carbonation technology using CO_2 released from cement industry).

Availability of Data and Materials
All the datasets associated with this study are available from the corresponding author upon request.

Declarations

Ethics Approval and Consent to Participate
All authors of the manuscript confirm the ethics approval and consent to participate following the Journal's policies.

Consent for Publication
All authors of the manuscript agree on the publication of this work in the International Journal of Concrete Structures and Materials.

Competing Interests
The authors declare no competing interest.

Received: 5 August 2023 Accepted: 30 December 2023
Published online: 17 April 2024

References

Alarcon-Ruiz, L., Platret, G., Massieu, E., & Ehrlacher, A. (2005). The use of thermal analysis in assessing the effect of temperature on a cement paste. *Cement and Concrete Research, 35*(3), 609–613.

Alyaseen, A., Poddar, A., Alahmad, H., Kumar, N., & Sihag, P. (2023). High-performance self-compacting concrete with recycled coarse aggregate: comprehensive systematic review on mix design parameters. *Journal of Structural Integrity and Maintenance*. https://doi.org/10.1080/24705314.2023.2211850

Bamigboye, G. O., Nworgu, A. T., Odetoyan, A. O., Kareem, M., Enabulele, D. O., & Bassey, D. E. (2020). Sustainable use of seashells as binder in concrete production: Prospect and challenges. *Journal of Building Engineering*. https://doi.org/10.1016/j.jobe.2020.101864

Basso, R. (1983). Crystal structure refinement of plazolite: a highly hydrated natural hydrogrossular.

Bayliss, P. (1989). Crystal chemistry and crystallography of some minerals within the pyrite group. *American Mineralogist, 74*(9–10), 1168–1176.

Bigare, M., Guinier, A., Mazieres, C., Regourd, M., Yannaquis, N., Eysbl, W., & Woermann, E. (1967). Polymorphism of tricalcium silicate and its solid solutions. *Journal of the American Ceramic Society, 50*(11), 609–619.

Brindley, G. W. (1945). XLV The effect of grain or particle size on x-ray reflections from mixed powders and alloys, considered in relation to the quantitative determination of crystalline substances by x-ray methods. *The London, Edinburgh, and Dublin Philosophical Magazine and Journal of Science, 36*(256), 347–369.

Buerger, M. (1937). Interatomic distances in marcasite and notes on the bonding in crystals of loellingite, arsenopyrite, and marcasite types. *Zeitschrift*

Für Kristallographie-Crystalline Materials. https://doi.org/10.1524/zkri.1937.97.1.504

Chaix-Pluchery, O., Pannetier, J., Bouillot, J., & Niepce, J. (1987). Structural pre-reactional transformations in Ca (OH) 2. *Journal of Solid State Chemistry, 67*(2), 225–234.

Chrysochoou, M., Grubb, D. G., & Fair, J. (2010). Evaluation of Two Aluminum Powders for Soil-Cement Applications. In *GeoFlorida 2010: Advances in Analysis, Modeling & Design* (pp. 2492–2501).

Colville, A., & Geller, S. (1971). The crystal structure of brownmillerite, Ca2FeAlO5. *Acta Crystallographica Section b: Structural Crystallography and Crystal Chemistry, 27*(12), 2311–2315.

Corazza, **E**., & Sabelli, C. (1967). The crystal structure of syngenite, K2Ca (SO4) 2·H2O. *Zeitschrift für Kristallographie-Crystalline Materials*, *124*(1), 398–408.

Courtial, M., De Noirfontaine, M.-N., Dunstetter, F., Gasecki, G., & Signes-Frehel, M. (2003). Polymorphism of tricalcium silicate in Portland cement: A fast visual identification of structure and superstructure. *Powder Diffraction, 18*(1), 7–15.

De la Torre, A. G., & Aranda, M. G. (2003). Accuracy in Rietveld quantitative phase analysis of Portland cements. *Journal of Applied Crystallography, 36*(5), 1169–1176.

De la Torre, A. G., Bruque, S., & Aranda, M. A. (2001). Rietveld quantitative amorphous content analysis. *Journal of Applied Crystallography, 34*(2), 196–202.

De La Torre, Á. G., Bruque, S., Campo, J., & Aranda, M. A. (2002). The superstructure of C3S from synchrotron and neutron powder diffraction and its role in quantitative phase analyses. *Cement and Concrete Research, 32*(9), 1347–1356.

De Noirfontaine, M.-N., Dunstetter, F., Courtial, M., Gasecki, G., & Signes-Frehel, M. (2006). Polymorphism of tricalcium silicate, the major compound of Portland cement clinker: 2. Modelling alite for Rietveld analysis, an industrial challenge. *Cement and Concrete Research, 36*(1), 54–64.

Dollase, W. (1986). Correction of intensities for preferred orientation in powder diffractometry: Application of the March model. *Journal of Applied Crystallography, 19*(4), 267–272.

Dongxu, L., Xuequan, W., Jinlin, S., & Yujiang, W. (2000). The influence of compound admixtures on the properties of high-content slag cement. *Cement and Concrete Research, 30*(1), 45–50.

Dunstetter, F., De Noirfontaine, M.-N., & Courtial, M. (2006). Polymorphism of tricalcium silicate, the major compound of Portland cement clinker: 1. Structural data: review and unified analysis. *Cement and concrete research*, *36*(1), 39–53.

Ermolovich, E., & Ermolovich, O. (2016). Effects of mechanical activation on the structural changes and microstructural characteristics of the components of ferruginous quartzite beneficiation tailings. *International Journal of Mining Science and Technology, 26*(6), 1043–1049.

Ferro, O., Galli, E., Papp, G., Quartieri, S., Szakáll, S., & Vezzalini, G. (2003). A new occurrence of katoite and re-examination of the hydrogrossular group. *European Journal of Mineralogy, 15*(2), 419–426.

Fiebich, K., & Mutz, M. (1999). Evaluation of calorimetric and gravimetric methods to quantify the amorphous content of desferal. *Journal of Thermal Analysis and Calorimetry, 57*(1), 75–85.

Goergens, J., Manninger, T., & Goetz-Neunhoeffer, F. (2020). In-situ XRD study of the temperature-dependent early hydration of calcium aluminate cement in a mix with calcite. *Cement and Concrete Research, 136*, 106160.

Gordon, R., & Harris, G. (1955). Effect of particle-size on the quantitative determination of quartz by X-ray diffraction. *Nature, 175*(4469), 1135–1135.

Gualtieri, M. L., Romagnoli, M., Miselli, P., Cannio, M., & Gualtieri, A. F. (2012). Full quantitative phase analysis of hydrated lime using the Rietveld method. *Cement and Concrete Research, 42*(9), 1273–1279.

Guirado, F., Galı, S., & Chinchón, S. (2000). Quantitative Rietveld analysis of aluminous cement clinker phases. *Cement and Concrete Research, 30*(7), 1023–1029.

Hazen, R. M. (1976a). Effects of temperature and pressure on the cell dimension and X-ray temperature factors of periclase. *American Mineralogist, 61*(3–4), 266–271.

Hazen, R. M. (1976b). Effects of temperature and pressure on the crystal structure of forsterite. *American Mineralogist, 61*(11–12), 1280–1293.

Hesse, C., Goetz-Neunhoeffer, F., & Neubauer, J. (2011). A new approach in quantitative in-situ XRD of cement pastes: Correlation of heat flow curves with early hydration reactions. *Cement and Concrete Research, 41*(1), 123–128.

Huang, J., Lu, J., Ran, G., Chen, N., & Qu, P. (2017). Formation of nanocrystalline and amorphization phase of Fe–Dy2O3 powder mixtures induced by ball milling. *Journal of Materials Research, 32*(3), 575–581.

Jansen, D., Stabler, C., Goetz-Neunhoeffer, F., Dittrich, S., & Neubauer, J. (2011). Does Ordinary Portland Cement contain amorphous phase? A quantitative study using an external standard method. *Powder Diffraction, 26*(1), 31–38.

Jeong, Y., Kang, S.-H., Kim, M. O., & Moon, J. (2020). Acceleration of cement hydration from supplementary cementitious materials: Performance comparison between silica fume and hydrophobic silica. *Cement and Concrete Composites, 112*, 103688.

Juhász, A. Z., & Opoczky, L. (1990). Mechanical activation of minerals by grinding pulverizing and morphology of particles.

Kumar, S., Bandopadhyay, A., Rajinikanth, V., Alex, T., & Kumar, R. (2004). Improved processing of blended slag cement through mechanical activation. *Journal of Materials Science, 39*(10), 3449–3452.

Lazić, B., Kahlenberg, V., Konzett, J., & Kaindl, R. (2006). On the polymorphism of CaAl2O4—structural investigations of two high pressure modifications. *Solid State Sciences, 8*(6), 589–597.

Le Saoût, G., Kocaba, V., & Scrivener, K. (2011). Application of the Rietveld method to the analysis of anhydrous cement. *Cement and Concrete Research, 41*(2), 133–148.

León-Reina, L., De la Torre, A., Porras-Vázquez, J., Cruz, M., Ordonez, L., Alcobé, X., & Fuellmann, T. (2009). Round robin on Rietveld quantitative phase analysis of Portland cements. *Journal of Applied Crystallography, 42*(5), 906–916.

Li, G., Yu, Y., Li, J., Wang, Y., & Liu, H. (2003). Experimental study on urban refuse/magnesium oxychloride cement compound floor tile. *Cement and Concrete Research, 33*(10), 1663–1668.

Maheswaran, S., Kalaiselvam, S., Karthikeyan, S. S., Kokila, C., & Palani, G. (2016). β-Belite cements (β-dicalcium silicate) obtained from calcined lime sludge and silica fume. *Cement and Concrete Composites, 66*, 57–65.

McGinnety, J. A. (1972). Redetermination of the structures of potassium sulphate and potassium chromate: The effect of electrostatic crystal forces upon observed bond lengths. *Acta Crystallographica Section B: Structural Crystallography and Crystal Chemistry, 28*(9), 2845–2852.

Mejdoub, R., Hammi, H., Khitouni, M., Suñol, J. J., & M'nif, A. (2017b). Effect of amorphization degree on mechanical and microstructural properties of portland cement paste. *Journal of Materials in Civil Engineering, 29*(6), 04017019.

Mejdoub, R., Hammi, H., Khitouni, M., Suñol, J. J., & M'nif, A. (2017a). The effect of prolonged mechanical activation duration on the reactivity of Portland cement: Effect of particle size and crystallinity changes. *Construction and Building Materials, 152*, 1041–1050.

Miller, S. A. (2018). Supplementary cementitious materials to mitigate greenhouse gas emissions from concrete: Can there be too much of a good thing? *Journal of Cleaner Production, 178*, 587–598.

Mitchell, L., Whitfield, P., & Beaudoin, J. (2007). The effects of particle statistics on quantitative Rietveld analysis of cement. Proceeding of the 12th International Congress on the Chemistry of Cement, Montreal, Paper No. TH1–08.3,

Mondal, P., & Jeffery, J. (1975). The crystal structure of tricalcium aluminate, Ca3Al2O6. *Acta Crystallographica Section B: Structural Crystallography and Crystal Chemistry, 31*(3), 689–697.

Mumme, W., Hill, R., Bushnell-Wye, G., & Segnit, E. (1995). Rietveld crystal structure refinements, crystal chemistry and calculated powder diffraction data for the polymorphs of dicalcium silicate and related phases.

Mumme, W. (1995). Crystal structure of tricalcium silicate from a Portland cement clinker and its application to quantitative XRD analysis. *Neues Jahrbuch Für Mineralogie-Monatshefte, 1995*(4), 146–160.

Naik, N., Jupe, A., Stock, S. R., Wilkinson, A., Lee, P., & Kurtis, K. (2006). Sulfate attack monitored by microCT and EDXRD: Influence of cement type, water-to-cement ratio, and aggregate. *Cement and Concrete Research, 36*(1), 144–159.

Nishi, F., & Takeuchi, Y. (1975). The A16O18 rings of tetrahedra in the structure of Ca8. 5NaAl6O18. *Acta Crystallographica Section b: Structural Crystallography and Crystal Chemistry, 31*(4), 1169–1173.

Nishi, F., Takéuchi, Y., & Maki, I. (1985). Tricalcium silicate Ca3O [SiO4]: the monoclinic superstructure. *Zeitschrift Für Kristallographie-Crystalline Materials*. https://doi.org/10.1524/zkri.1985.172.14.297

Parry-Jones, G., Al-Tayyib, A., & Al-Mana, A. (1988). Evaluation of degree of hydration in concrete using 29Si magic angle spinning NMR in solids. *Cement and Concrete Research, 18*(2), 229–234.
Peterson, V. K., Ray, A. S., & Hunter, B. A. (2006). A comparative study of Rietveld phase analysis of cement clinker using neutron, laboratory X-ray, and synchrotron data. *Powder Diffraction, 21*(1), 12–18.
Phillips, E. M. (1997). An approach to estimate the amorphous content of pharmaceutical powders using calorimetry with no calibration standards. *International Journal of Pharmaceutics, 149*(2), 267–271.
Pourghahramani, P., & Akhgar, B. (2015). Characterization of structural changes of mechanically activated natural pyrite using XRD line profile analysis. *International Journal of Mineral Processing, 134*, 23–28.
Pourghahramani, P., & Forssberg, E. (2006). Microstructure characterization of mechanically activated hematite using XRD line broadening. *International Journal of Mineral Processing, 79*(2), 106–119.
Radoi, R., Danila, M., Fernandez, P., & Piqueras, J. (2004). Mean crystallite size, size distribution and root mean square residual microstrain measurement from X-ray line broadening of milled ZnSe nano-powders. 2004 International Semiconductor Conference. CAS 2004 Proceedings (IEEE Cat. No. 04TH8748),
Ren, X., Zhang, W., & Ye, J. (2017). FTIR study on the polymorphic structure of tricalcium silicate. *Cement and Concrete Research, 99*, 129–136.
Sakai, E., Miyahara, S., Ohsawa, S., Lee, S.-H., & Daimon, M. (2005). Hydration of fly ash cement. *Cement and Concrete Research, 35*(6), 1135–1140.
Scarlett, N. V., Madsen, I. C., Cranswick, L. M., Lwin, T., Groleau, E., Stephenson, G., & Agron-Olshina, N. (2002). Outcomes of the international union of crystallography commission on powder diffraction round robin on quantitative phase analysis: Samples 2, 3, 4, synthetic bauxite, natural granodiorite and pharmaceuticals. *Journal of Applied Crystallography, 35*(4), 383–400.
Scarlett, N. V., Madsen, I. C., Manias, C., & Retallack, D. (2001). On-line X-ray diffraction for quantitative phase analysis: Application in the Portland cement industry. *Powder Diffraction, 16*(2), 71–80.
Scrivener, K., Füllmann, T., Gallucci, E., Walenta, G., & Bermejo, E. (2004). Quantitative study of Portland cement hydration by X-ray diffraction/Rietveld analysis and independent methods. *Cement and Concrete Research, 34*(9), 1541–1547.
Shafi, K., Gedanken, A., Goldfarb, R. B., & Felner, I. (1997). Sonochemical preparation of nanosized amorphous Fe-Ni alloys. *Journal of Applied Physics, 81*(10), 6901–6905.
Shah, M. U., Usman, M., Khushnood, R. A., & Hanif, A. (2023). Diagnosis of durability-related problems in concrete structures through comprehensive analysis and non-destructive testing: A case study. *Journal of Structural Integrity and Maintenance, 8*(4), 260–270.
Shanahan, N., & Zayed, A. (2007). Cement composition and sulfate attack: Part I. *Cement and Concrete Research, 37*(4), 618–623.
Sheng, J., Rane, G., Welzel, U., & Mittemeijer, E. (2011). The lattice parameter of nanocrystalline Ni as function of crystallite size. *Physica E: Low-Dimensional Systems and Nanostructures, 43*(6), 1155–1161.
Shi, Z., Geiker, M. R., De Weerdt, K., Østnor, T. A., Lothenbach, B., Winnefeld, F., & Skibsted, J. (2017). Role of calcium on chloride binding in hydrated Portland cement–metakaolin–limestone blends. *Cement and Concrete Research, 95*, 205–216.
Smyth, J. R. (1975). High temperature crystal chemistry of fayalite. *American Mineralogist: Journal of Earth and Planetary Materials, 60*(11–12), 1092–1097.
Snellings, R., Machiels, L., Mertens, G., & Elsen, J. (2010). Rietveld refinement strategy for quantitative phase analysis of partially amorphous zeolitized tuffaceous rocks. *Geologica belgica*.
Snellings, R., Bazzoni, A., & Scrivener, K. (2014). The existence of amorphous phase in Portland cements: Physical factors affecting Rietveld quantitative phase analysis. *Cement and Concrete Research, 59*, 139–146.
Steinfink, H., & Sans, F. (1959). Refinement of the crystal structure of dolomite. In: Mineralogical Society of America.
Stutzman, P. E., Feng, P., & Bullard, J. W. (2016). Phase analysis of Portland cement by combined quantitative X-ray powder diffraction and scanning electron microscopy. *Journal of Research of the National Institute of Standards and Technology, 121*, 47–107.
Suherman, P. M., van Riessen, A., O'Connor, B., Li, D., Bolton, D., & Fairhurst, H. (2002). Determination of amorphous phase levels in Portland cement clinker. *Powder Diffraction, 17*(3), 178–185.
Sun, Z., & Vollpracht, A. (2018). Isothermal calorimetry and in-situ XRD study of the NaOH activated fly ash, metakaolin and slag. *Cement and Concrete Research, 103*, 110–122.
Taylor, J., Aldridge, L., Matulis, C., & Hinczak, I. (2002). X-ray powder diffraction analysis of cements. *Structure and performance of cements*, 420–441.
Toby, B. H. (2006). R factors in Rietveld analysis: How good is good enough? *Powder Diffraction, 21*(1), 67–70.
Tran, D. V. P., Sancharoen, P., Klomjit, P., Tangtermsirikul, S., & Nguyen, T. H. Y. (2023). Prediction equations for corrosion rate of reinforcing steel in cement-fly ash concrete. *Journal of Structural Integrity and Maintenance, 8*(2), 91–99.
Uvarov, V., & Popov, I. (2007). Metrological characterization of X-ray diffraction methods for determination of crystallite size in nano-scale materials. *Materials Characterization, 58*(10), 883–891.
Walenta, G., & Füllmann, T. (2004). Advances in quantitative XRD analysis for clinker, cements, and cementitious additions. *Powder Diffraction, 19*(1), 40–44.
Wang, H. (1994). Step size, scanning speed and shape of X-ray diffraction peak. *Journal of Applied Crystallography, 27*(5), 716–722.
Whitfield, P., & Mitchell, L. (2009). The effects of particle statistics on Rietveld analysis of cement. *Zeitschrift Für Kristallographie*. https://doi.org/10.1524/zksu.2009.0008
Xie, T., & Visintin, P. (2018). A unified approach for mix design of concrete containing supplementary cementitious materials based on reactivity moduli. *Journal of Cleaner Production, 203*, 68–82.
Yang, H., & Prewitt, C. T. (1999). On the crystal structure of pseudowollastonite (CaSiO3). *American Mineralogist, 84*(5–6), 929–932.
Young, R. (1993). *The rietveld method* (Vol. 5).

Publisher's Note

Hyunuk Kang Graduate student in the Department of Civil and Environmental Engineering at Seoul National University.

Jihoon Lee Graduate student in the Department of Civil and Environmental Engineering at Seoul National University.

Jun-Boum Park Professor in the Department of Civil and Environmental Engineering at Seoul National University.

Juhyuk Moon Associate Professor in the Department of Civil and Environmental Engineering at Seoul National University.